International Journal of Signal Processing, Image Processing and Pattern Recognition
Vol.9, No.4 (2016), pp.1-10
http://dx.doi.org/10.14257/ijsip.2016.9.4.01

Fusion for Medical Images based on Shearlet Transform and Compressive Sensing Model

Niu Ling and Duan Mei-Xia

Zhou Kou Normal University, Zhoukou 466001, China
North China University of Water Resources and Electric Power, Zhenzhou 450011, China
suncoco_nl@163.com, Duanmeixia@ncwu.du.cn

Abstract

Faced with the poor ability of traditional transform domain tools to capture the image information and the high requirements on the precision and real-time of medical imaging, a novel fusion technique for medical images based on shearlet transform (ST) and compressive sensing (CS) model is proposed in this paper. Due to the better competence of image information capturing, ST is utilized to conduct the multi-scale and multi-directional decompositions of source images. In addition, the measurement matrix is adopted to realize the sparse representation of the high-frequency coefficients obtained from ST. The fusion data of high-frequency sub-images can be attained via the largest-value method. Finally, the final fused image can be obtained by using inverse ST. Compared with current typical techniques especially the non-negative matrix factorization based ones; simulation experimental demonstrates that the proposed one has remarked superiorities in terms of both subjective and objective evaluations.

Keywords: *shearlet transform, compressive sensing, image fusion, medical image*

1. Introduction

Research on imaging technology has been widely applied in the medical field. Recently, current categories of medical images mainly include computed tomography (CT), magnetic resonance imaging (MRI), and so on. Both CT and MRI are able to detect and imaging the physical locations of creatures. However, the differences between these two imaging technologies result in a great deal of redundant and complementary information existing in CT and MRI images. As a result, appropriately fuse various medical images with different imaging mechanism to extract respective priority information, and then fuse it into a single image to enhance the showing precision and real-time property has been a hot issue in the area of medical image processing.

Recently, on the one hand, a great number of fusion techniques for images have been proposed by scholars both at home and abroad, in which the most representative techniques are based on the idea of transform domain. At the end of the last century, the wavelet transform (WT) [1, 2] replaced the pyramid transform to be the mainstream fusion technique for images. However, the better capture performance of WT can only be achieved in terms of horizontal, vertical and diagonal directions; furthermore, the singular information of lines cannot be captured. Several years later, several other transform domain techniques for image fusion, such as ridgelet transform [3], curvelet transform [4, 5] and contourlet transform [6, 7], appear in succession so that the fusion property has been greatly enhanced. Compared with the former patterns, shearlet transform (ST) [8-10] has obvious priorities in terms of both information capturing and computational complexity, so it gradually becomes the mainstream and a hot research object in the field of image fusion, and has been widely used in a variety of areas, *e.g.*, image fusion and image feature extraction.

ISSN: 2005-4254 IJSIP

On the other hand, Donoho *et al.*, [11, 12] proposed a novel theory model called compressive sensing (CS) in 2006. CS thoroughly overthrows the traditional Nyquist sampling theory, and attracts a lot of attentions [13-15] from the corresponding fields. CS provides a novel concept to us in terms of information reconstruction of images. In nature, a much more sparse representation of the original sparse signal can be obtained with the measurement matrix. Then, the original signal can be well restored. As a result, the idea of CS is consistent with that of transform domain techniques for image fusion.

Based on the above, a novel technique for medical image fusion based on ST and CS is proposed in this paper. Firstly, the multi-scale and multi-directional decompositions of source images can be conducted to produce a low-frequency sub-image and a series of high-frequency sub-images. Then, the further sparseness deposition of high-frequency coefficients from ST can be done with the measurement matrix in CS. The reconstruction of high-frequency data can be obtained according to the "Max" method. Finally, the inverse ST is adopted to produce the final fusion resultant image.

2. Basic Theories

2.1. ST Basic Model [8-10]

Guo constructed the affine system model and proposed its expression in the case of n=2:

$$M_{XY}(\varphi) = \{\varphi_{a,b,c}(x) = |\det X|^{a/2} \psi(Y^b X^a x - c) : a, b \in Z, c \in Z^2\} \quad (1)$$

In the above formula, $\varphi \in L^2(R^2)$, X and Y are both 2×2 invertible matrix, $|\det Y|=1$. If $M_{XY}(\varphi)$ is satisfied with tight frame conditions, then the elements of $M_{XY}(\varphi)$ is regarded as wavelet synthesis. X is an anisotropy expansion matrix, and X^a is related to scale transformation. Y is a shear matrix, and Y^b is also a shear matrix that is related to geometric transformation for keeping area constant. The formulas of X and Y are respectively regarded as X=[a 0, 0 $a^{1/2}$], Y=[1 s, 0 1]. In general, a=4, s=1, that is be X=[4 0, 0 2], Y=[1 1, 0 1]. Thus the above wavelet is shearlet.

Let $L^2(R^2)$ satisfy the following condition:

$$\varphi^*(\zeta) = \varphi^*(\zeta_1, \zeta_2)\varphi_1^*(\zeta_1)\varphi_2^*(\zeta_1 / \zeta_2) \quad (2)$$

φ^* denotes the Fourier transform of function φ, and φ_1 and φ_2 satisfiy that:

$$sub\varphi_1^* \in [-2, -\frac{1}{2}] \cup [\frac{1}{2}, 2] \quad (3)$$

$$sub\varphi_2^* \in [-1, 1] \quad (4)$$

Each shearlet locates in a pair of trapeziform zones with, whose sizes all approximate to $2^{2j}\times 2^j$, which is shown in Figure 1(a). Based on the WT theory, the 2D wavelet transform basis from the 1D one has square support interval, and its approximate length of a side is 2j, as shown in Figure 1(b). If the scale j grows, the area of the WT support basis increases also. However, owning to the no-directional property, the non-zero wavelet coefficients grow in the form of exponential form so that a number of ignorable coefficients appear. Approximate singular curves of WT characterize not the optimal sparseness representation but the "point" approximate course. Shearlets utilize the rectangle-like namely trapeziform pairs to approximate curves. As a result, if the scale j grows,

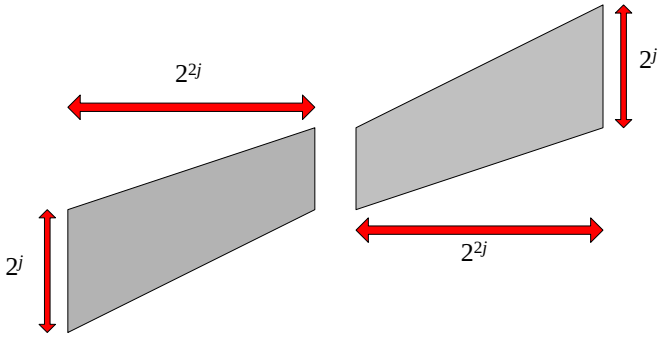

(a) ST ladder-shaped Support Zone

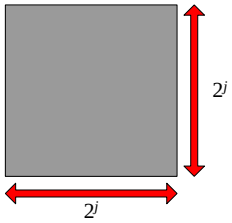

(b) 2 Dimension Discrete Wavelet Support Zone

Figure 1. ST and 2 Dimension Discrete Wavelet Support Zone

2.2. Basic Compressive Sensing Model [11, 12]

Suppose a real-valued, finite length and one dimensional discrete time signal $\boldsymbol{x}$, the elements in $\boldsymbol{x}$ are denoted as x[n], and n satisfies the relation $1 \leq n \leq N$. If $\boldsymbol{x}$ satisfies the following equation:

$$\boldsymbol{x} = \boldsymbol{\Psi}\boldsymbol{\alpha} \tag{5}$$

Where $\boldsymbol{\Psi}$ is a $N \times N$ basis matrix and $\boldsymbol{\alpha}$ is a $N \times 1$ vector containing only K non-zero coefficients. Clearly, $\boldsymbol{x}$ and $\boldsymbol{\alpha}$ are equivalent representations of the signal, with $\boldsymbol{x}$ in the time or space domain and $\boldsymbol{\alpha}$ in the $\boldsymbol{\Psi}$ domain. The sparseness representation of the signal is shown in Figure 2.

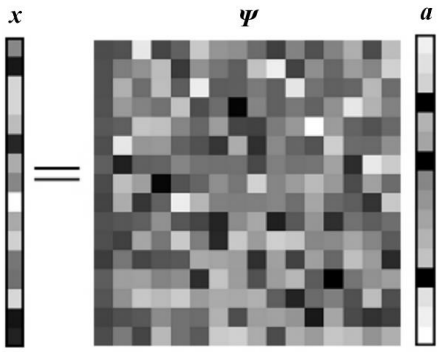

Figure 2. Sparseness Representation of the Signal

3. Medical image Fusion based on ST and CS Model

3.1. Image Fusion Basic Model

The basic progress and several key thinking for medical image fusion technique based on ST and CS models are as follows.

(1) The original fusion images are decomposed according to multi-scale and multi-direction by means of ST transform-domain theory model aiming at acquiring a low-frequency microcosmic subband image and a series of high-frequency microcosmic subband images. The above low-frequency microcosmic subband images contain the main information from original fusion images. Furthermore, for not assuring the sparse of coefficients, low-frequency microcosmic subband images can't utilize CS model to carry out. In contrast, for the high-frequency microcosmic subband images' advantage of stressing on describing original images' details and marginal information and having sparser coefficients, we can effectively utilize CS model.

(2) For linear mapping high-frequency microcosmic subband images information, we must design a set of good measuring matrix for use;

(3) Measuring fusion data obtained are always reconstructed so that the fusion progress of high-frequency microcosmic subband images can be accomplished.

(4) The ending fusion images can be obtained by ST inverse transform with high-frequency and low-frequency microcosmic subband fusion images.

For a simple research, we assume two medical original images for fusion *A* and *B*, which are strictly matched. Low-frequency microcosmic coefficient $\{A^{S,0}, B^{S,0}\}$ and high-frequency microcosmic coefficient $\{A^{S,L}, B^{S,L}\}$ can be obtained by ST decomposition. In above, *S* is dimension grade and *L* is direction decomposed grade of *S*. low and high are respectively represented as the departments of low-frequency microcosmic subband fusion images and high-frequency microcosmic subband fusion images.ST and *F* are represented as shear wavelet transform and ending fusion images. The entire progress of medical images fusion based on ST and CS models is clearly showed in Figure 3.

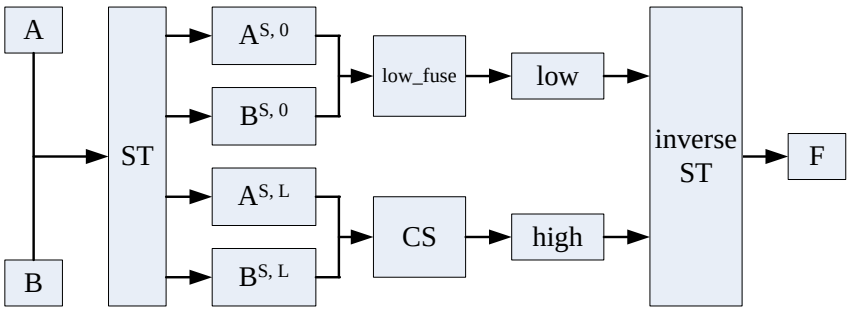

Figure 3. Medical Images Fusion Progress based on ST and CS Model

3.2. Low-frequency Microcosmic Subband Image Fusion

Classic fusion algorihms have always carried out by doing adding and averaging some low-freuqency subband images' matrix. However, the aforementioned easy computations for those algorithms can result in deceasing overall images' contrast ratio, additionally, pixel distribution characteristic is so ill-considered in every low-frequency subband images.

Comparing with the pixel points' information around, the pixel grey level of on images' important target information have an obvious difference. And Spatial frequency (SF) [16] shows pixel point's active degree on images.

Thus in the proposed technique we make use of SF as low-frequency microcosmic subband images fusion basis. And the formula of SF is as follows.

$$SF = \sqrt{(RF)^2 + (CF)^2 + (MDF)^2 + (SDF)^2} \tag{6}$$

As for image $I(i, j)$, the formulas of *RF*, *CF*, *MDF* and *SDF* are respectively as follows.

$$RF = \sqrt{\frac{1}{MN}\sum_{i=1}^{M}\sum_{j=2}^{N}[I(i,j)-I(i,j-1)]^2} \tag{7}$$

$$CF = \sqrt{\frac{1}{MN}\sum_{j=1}^{N}\sum_{i=2}^{M}[I(i,j)-I(i-1,j)]^2} \tag{8}$$

$$MDF = \sqrt{\omega_d \frac{1}{MN}\sum_{i=2}^{M}\sum_{j=2}^{N}[I(i,j)-I(i-1,j-1)]^2} \tag{9}$$

$$SDF = \sqrt{\omega_d \frac{1}{MN}\sum_{j=1}^{N-1}\sum_{i=2}^{M}[I(i,j)-I(i-1,j+1)]^2} \tag{10}$$

In the above formulas, *RF*, *CF*, *MDF* and *SDF* are represented as first order gradient values from four different directions such as horizontal direction, vertical direction, main diagonal direction and diagonal direction. ω_d is represented as distance weighted values, setting to be $1/2^{1/2}$ here.

Obviously, each pixel point's *SF* value can easily compute according to formula (7)-(10). The bigger *SF* value indicates the more active and outstanding pixel point in the surrounding four directions', and shows more affluent information contained the pixel point. The selection normal of low-frequency coefficient is showed in the formula (11) as follows.

$$F\_low^{S,0} = \begin{cases} A^{S,0}, & if \quad SF_A(i,j) > SF_B(i,j) \\ B^{S,0}, & if \quad SF_A(i,j) < SF_B(i,j) \\ \dfrac{A^{S,0}+B^{S,0}}{2}, & if \quad SF_A(i,j) = SF_B(i,j) \end{cases} \tag{11}$$

3.3. High-frequency microcosmic subband image fusion

High-frequency microcosmic subband images' coefficients stress always on describing their detailed marginal information. But comparing with low-frequency microcosmic subband images' coefficients, high-frequency images' coefficients are often sparser. Namely, the kind of coefficient close to 0 is a great amount, which is appropriate to CS model, with its concrete steps as follows.

(1) Construct measuring matrix $\boldsymbol{\Phi}$ and linear map high-frequency microcosmic subband images coefficients $A^{S,L}$, $B^{S,L}$ to obtain corresponding measuring values $Y(A^{S,L})$, $Y(B^{S,L})$;

(2) Obtain fusion values based on maximum principle according to formula (12) as follows.

$$\max(Y(A^{S,L}), Y(B^{S,L})) \tag{12}$$

(3) Reconstruct high-frequency microcosmic subband images fusion coefficients for using first-order norm.

4. Experimental Results and Analysis

For verifying the practical performance of the proposed technique, we utilize two pairs of medical images as fusing original images to carry out the simulation experiments. Then we choose WINDOWS 7 systems and MATLAB 2012 to emulate, compare and analyze the fusion results of several compared fusion techniques and the proposed technique.

4.1. Experiments Introduction

In this section, we select two pairs of original images each with 256 grey level and 512×512 pixel, showed in Figure 4. In the first pairs of the fusion images, a CT image in the left is always expert at catching skeleton information, and a MRI image in the right is sensitive to musculature information. Above all, if CT and MRI images can be effectively fused, we must substantially improve the ability of catching information for providing patients with a better therapy basis. Additionally, the second pair of the fusion images are respectively a diffusion weighted medical image and a liquid decay inversed image. The two above images are respectively confronted to the brain objects with different precision. Obviously, the two above images also contain the great amount of complementary information.

In the emulation fusion experiment, the parameters in the novel technique are set as follows: Multi-scale decomposition series of ST is set as 3, and direction decomposition series from coarse to slender are respectively set as 10, 10 and 18. Low-frequency microcosmic subband image fusion can take SF as the standard. Additionally, high-frequency microcosmic subband image fusion is carried on based on CS model corresponding to maximum value principle. Compared with the proposed technique, we select three different techniques which are image fusion technique based on ST presented by Miao (Technique 1)[8], the another analogous technique proposed by Feng Xin (Technique 2) [10] and image fusion technique combined with NMF and a new contourlet transform (Technique 3)[6]. For assuring the impartiality and objectivity of fusion effect, the referred parameters of technique 1 and technique 3 are set as the former values in their references. Except for subjective evaluation, we choose the other three evaluating indicators including IE[17], MI[17] and SF[17]. IE numerical characterization images contain amount of information. And the bigger are the values, the information are richer in the fusion images. The values of MI can reflect their mutual information between the ending fusion images and original images, that is to say, the bigger are values of MI, the ampler are the original information referred to original images in the fusion images. In a certain extent, SF can always reflect active degree at each pixel in the fusion images. And the values of SF are bigger, significant information contained in the fusion images are more affluent. The details of IE, MI and SF can be consulted in the reference [16].

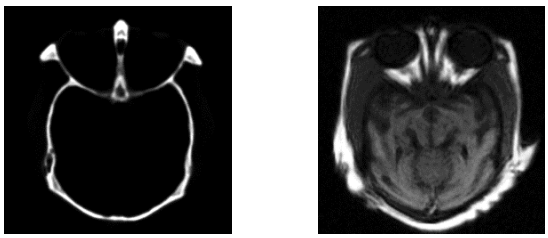

(a) CT Image (b) MRI Image

(c) Diffusion Weighted Image (d) Liquid Decay Inversed Image

Figure 4. Medical Original Images

4.2. Experimental Results and Analysis

The simulation experimental results for two groups of medical original images are clearly showed in Figure 5 and Figure 6.

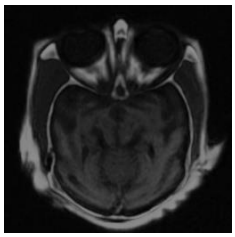

(a) Fusion Results of Technique 1

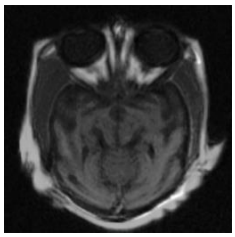

(b) Fusion Results of Technique 2

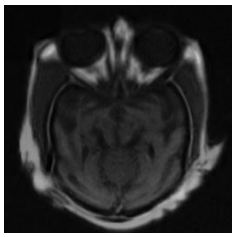

(c) Fusion Results of Technique 3

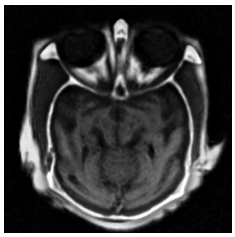

(d) Fusion Results of the Proposed Technique

Figure 5. The First Group of Original Image Fusion Effect

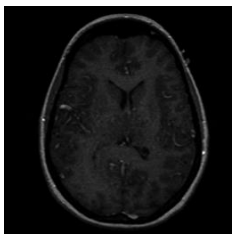

(a) Fusion results of technique 1

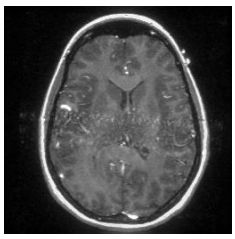

(b) Fusion results of technique 2

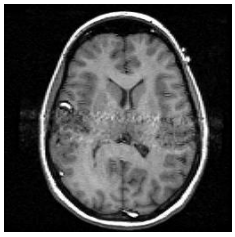

(c) Fusion results of technique 3

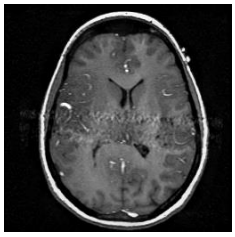

(d) Fusion results of the proposed technique

Figure 6. The Second Group of Original Image Fusion Effect

The experimental results indicate clearly that above four techniques can effectively fused the subject information of original images, yet the performance on detailed expression of images can represent obvious differences. It is so easy to find that marginal information is very fuzzy in the fusion results of technique 2 and technique 3. In contrast, more affluent and specific information can be obtained respectively corresponding to technique 1 and the novel technique. Furthermore, the fusion result for technique 1 always possesses lower contrast ratio of overall image than the presented technique's. In Figure 6, brain ridge texture information of technique 1 and technique 3 are fuzzier than the novel technique. Similarly, the

visual effect on technique 1 and 3 are both poorer than the presented technique's ending fusion effect.

In two groups of fusion experiments, evaluation results obtained corresponding to three objective evaluation indicators including IE, MI, SF are showed in Table 1. The experimental results indicate clearly that the fusion results of technique 1 have an obvious advantage than technique 2 and 3 referred also to IE, MI, SF. Furthermore, it is obviously showed that the fusion images of technique 1 have more affluent information and more active degree than others'. Therefore, it is no doubt that the novel technique possesses better objective indicators' results, that is to say, all the evaluation indicators such as amount of information, mutual information and space frequency have more superiority than other three techniques. Obviously, objective evaluation results and subjective visual evaluation results are effectively consistent.

Table 1. Comparison of Objective Indicators' Values based on Four Techniques

	The first group of fusion experiments			The second group of fusion experiment		
	IE	MI	SF	IE	MI	SF
Technique 1	6.909	0.457	47.315	6.773	0.658	59.398
Technique 2	6.723	0.384	43.183	6.532	0.612	57.628
Technique 3	6.477	0.335	45.048	6.420	0.593	54.984
The proposed technique	**7.016**	**0.518**	**59.539**	**6.931**	**0.708**	**63.877**

Above all, we have compared and analyzed subjective and objective fusion performances on four fusion techniques certainly including the proposed technique by carrying on the experiments with two groups of medical original images. Thus we can deeply analyze and discuss the above experimental results and their using techniques.

(1) Technique 1 and technique 2 both referred to ST theory, but their fusion effects are different because two techniques have used so different fusion rules.

(2) Non-negative matrix factorization (NMF) and new contourlet transform (NCT) are simultaneously introduce in Technique 3. And NMF theory and CS model are both attributed to matrix solving ideas in mathematics field so that they have good performances on image processing. However, practical application effects of classic NMF theory depend greatly on initial values' setting, causing experimental results to always be volatility. Comparatively, CS model can undistorted reconstruct original once their signal measuring matrix can satisfy with RIP rules. Therefore, the proposed fusion effect is better than classic NMF model's effect.

(3) Time complexity is also an important and significant indicator in the practical application. The above four fusion techniques' average running time are showed in Table 2 with units. Four techniques' running time is sorted from large to small and our novel technique is in second, which is strongly showed its good timeliness.

Table 2. Comparison of Average Running Time based on Four Techniques

Technique 1	Technique 2	Technique 2	Proposed
3.267	2.786	3.179	2.963

5. Conclusion

On the basis of the combination between ST theory and CS model, a novel technique for medical image fusion has been proposed. Owing to absorbing the outstanding superiority from CS model, the performance on sparse signal reconstruction has been successfully applied into the fusion progress of high-frequency microcosmic subband images. Furthermore, in the simulation experiment, we have selected two groups of medical original images. And the experimental results and analysis has stated clearly that the presented technique have been significant advantages of both visual effect and objective evaluation results. Importantly, the improvement on the proposed technique and the promotion of its performance must be our next works' focal point and research direction.

Acknowledgments

The authors thank the anonymous reviewers and editors for their invaluable suggestions. The work was supported in part by the Key scientific research projects of Henan Province of China under Grant 16A520104, in part by the Science and technology project of Henan Province of China under Grant 152102210367, in part by the soft science research project of Henan province of China under Grant 142400411133.

References

[1] Y. Wang, M. Q Wang. Study of infrared and visible image fusion technology based on wavelet transform, Infrared, 34(3), 12-14 **(2013)**.
[2] B. Liu, W. J. Liu and J. X. Peng. Fusion of infrared and visible images based on three channel nonseparable symmetrical wavelets, Infrared and Laser Engineering, 40(5): 974-979 **(2011)**.
[3] Z. Y. Zhao and Y. G. Zheng. Research of image fusion of multispectral and panchromatic images based on ridgelet transform, Computer Engineering and Applications, 48(15): 164-167 (2012).
[4] J. C. Zhao and S. R. Qu. A better algorithm for fusion of infrared and visible image based on curvelet tran sform and adaptive pulse coupled neural networks, Journal of Northwestern Polytechnical University, 29(6): 849-853 (2011).
[5] Q. Xue, Y. Fan, H. Z. Li, et al. Infrared and visible images fusion algorithm based on curvelet transform, Computer Engineering, 37(3): 224-226 (2011).
[6] F. Wang, X. G. Liang, Y. K. Cui, et al. Image fusion combined with NMF and a new contourlet transform, Computer Engineering and Applications, 49(5): 150-153.2 (2013)
[7] J. W. Mo, A. H..Ma, Z. Y. Shou, et al. Multifocus image fusion algorithm based on Brenner function and a new contourlet transform, Journal of Computer Applications, 32(12): 3353-3356 (2012)
[8] Q. G. Miao, C. Shi, P. F. Xu, et al. A novel algorithm of image fusion using shearlets, Optics Communications, 284(6): 1540-1547 (2011)
[9] H. C. Zheng, Zheng, X. S. Yan, et al. Visible and infrared image fusion algorithm based on shearlet transform, Chinese Journal of Scientific Instrument, 33(7): 1613-1619 (2012)
[10] X. Feng, X. M. Wang, J. W. Dang, et al. Fusion of infrared and visible images based on shearlet transform, Journal of Optoelectronics Laser, 24(2): 384-390 (2013)
[11] E. J. Candes, J. Romberg and T. Tao. Robust uncertainty principles: Exact signal reconstruction from highly incomplete frequency information, IEEE Transactions on Information Theory, 52(2): 489-509 (2006)
[12] E. J. Candes and T. Tao. Near-optimal signal recovery from random projection: Universal encoding strategies, IEEE Transactions on Information Theory, 52(12): 5406-5425 (2006)
[13] M. Ding, L. Wei and B. F. Wang. Research on fusion method for infrared and visible images via compressive sensing, Infrared Physics & Technology, 57(1): 56-67 (2013)
[14] Z. D. Liu, H. P. Yin, B. Fang and Y. Chai. A novel fusion scheme for visible and infrared images based on compressive sensing, Optics Communications, 335(2): 168-170 (2015)
[15] X. Li and S. Y. Qin. Efficient fusion for infrared and visible images based on compressive sensing principle, IET Image Processing, 5(2): 141-1479 (2011)
[16] Y. Zheng, E. A. Essock, B. C. Hansen et al.. A new metric based on extended spatial frequency and its application to DWT based fusion algorithms, Information Fusion, 8(2): 177-1929 (2007)

[17] Liu Z., Blasch E., Xue Z. Y., et al.. Fusion algorithms for context enhancement in night vision: a comparative study, IEEE Transactions on Pattern Analysis and Machine Intelligence, 34(1): 94-109 (2012)

Authors

Niu Ling, received the B. Eng degree in Computer science from Henan normal university and M. Eng degree in Computer science from Chengdu University of Technology. She is currently researching on computer application technology.

Duan Mei Xia, received the B. Eng degree electronic technology in from Henan normal university and M. Eng degree in Computer science from Chengdu University of Technology. She is currently researching on embed system and measure.

